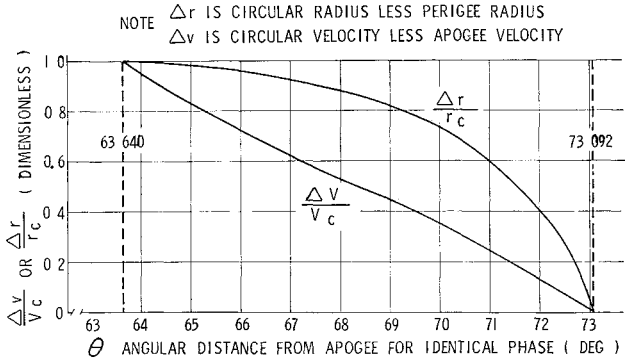

Fig 1 Location of "catch-up" point for retrograde ΔV

Taking the limit of the foregoing expression as $\chi = (\Delta r/2r) \rightarrow 0$ gives the following limiting catch-up point as $\Delta V \rightarrow 0$†:

$$\theta_c = \tfrac{4}{3} \sin\theta \tag{7}$$

The solution of Eq (7) is $\theta = 73\,092°$ It can be easily shown that the same limit [Eq (7)] is reached when the ellipse is initially larger than the circle (i e , ΔV is along the circular velocity in a positive sense) and is allowed to approach the circle

As ΔV approaches retrograde circular velocity, the resulting ellipse approaches a rectilinear ellipse The true anomaly in such a limiting ellipse approaches 180° at all points except at the force center where the rate of change of true anomaly approaches infinity Therefore, for this case, the catch-up point will obviously occur when the perturbed body is at the force center The time required for the body to reach the force center is one-half its period and is given by

$$t = \frac{\pi a^{3/2}}{\mu^{1/2}} = \frac{\pi(r/2)^{3/2}}{\mu^{1/2}} \tag{8}$$

During this time, the body in the circular orbit travels through an angle given by

$$\theta = (\mu^{1/2}/r^{3/2})t \tag{9}$$

Combining (8) and (9) and solving for θ yields

$$\theta = \pi/2^{3/2} \tag{10}$$

or

$$\theta = 63\,640°$$

The procedure for finding the catch-up point for a Δr (or ΔV) between the extremes just analyzed is first to estimate the catch-up θ_E and form the true anomaly of the ellipse [Eq (3)] Next, the corresponding eccentric anomaly is found, and, consequently, the time from apogee is found from an appropriate form of Kepler's equation The circular travel θ is then found from (9), and the difference $(\theta - \theta_E)$ is added to the original estimate of θ_E to form a new estimate The process is repeated until $(\theta - \theta_E)$ is sufficiently small to be called zero

Figure 1 is a plot of the angular distance from apogee of the catch-up points as functions of $(\Delta r/r)$ and $(\Delta V/V)$ for retrograde ΔV's

References

[1] Karrenberg H K Levin, E , and Lewis, D H , Variation of satellite position with uncertainties in the mean atmospheric density," ARS J **32**, 576–582 (1962)

[2] Moulton, F R , *An Introduction to Celestial Mechanics* (The MacMillan Co , New York, 1914), pp 169–171

† It can be seen from Eq (2) that, for small χ $\Delta V/V_c \approx \pm\chi/2 = \pm\Delta r/4r_c$, and therefore $\Delta V \rightarrow 0$ as $\chi \rightarrow 0$

Drag Minimization Using Exact Methods

Sidney A Powers*
Northrop Corporation, Hawthorne, Calif

A method of determining optimum solutions to nonlinear problems has been used to determine a minimum drag body of revolution for $M = 7$ at sea level It is shown that the drag of the basic spherical-$\frac{3}{4}$ power-law body can be reduced significantly by using a very small sphere and making the body somewhat "fatter" than a $\frac{3}{4}$ power-law body

A METHOD of treating nonlinear optimization problems has been discussed previously in detail in Ref 1 This method is applied here to the problem of determining the minimum drag body of revolution for a freestream Mach number of 7 0 at sea level The flow field is taken as inviscid and in chemical equilibrium

The configuration is required to have a nominal fineness ratio of 4 0 and a spherical nose The optimum size of the hemisphere and the contour of the afterbody are to be determined As a "basic" shape, a body of unit length was used which had a sphere tangent to a $\frac{3}{4}$ power-law afterbody at the 0 05 body length point

Between the sphere-body tangency point and the body base, a polynomial pertubation was added to the basic body:

$$\Delta y = A\xi^4 + B\xi^3 + C\xi^2 + D\xi + E \tag{1}$$

where

$$\xi = (X - X_T)/(X_{\max} - X_T)$$

and X_T is the sphere-body tangency point The following boundary conditions were imposed on Eq (1):

$$\begin{aligned} \Delta y &= 0 \quad \text{at } \xi = 0 \\ \Delta y &= 0 \quad \text{at } \xi = 1 \\ \Delta y' &= 0 \quad \text{at } \xi = 0 \end{aligned}$$

Reference 2 describes in detail the method of determining the functional relation of drag on the sphere-body tangency point and the pertubation polynomial Briefly, the boundary conditions just given make it possible to split the pertubation

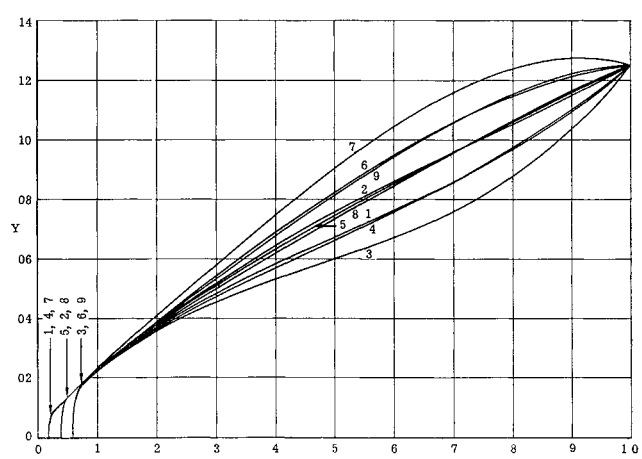

Fig 1 Body shapes specified by the Latin Square

Received September 23, 1963; revision received January 29, 1964

* Member of Technical Management, Gas Dynamics Branch, Norair Division Member AIAA

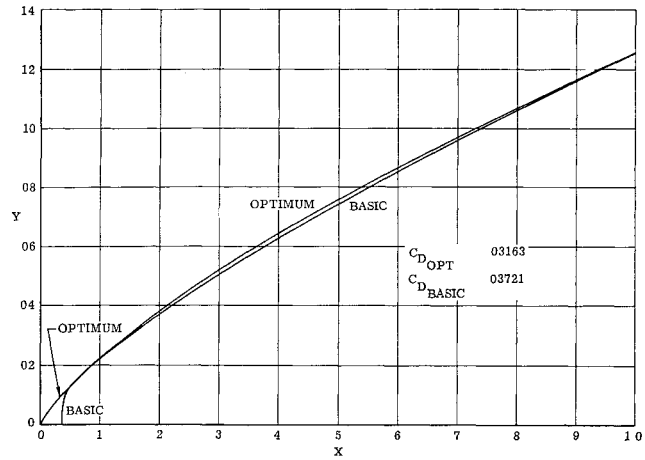

Fig 2 Comparison of the optimum body with the basic body

polynomial into two parts, Δy_1 and Δy_2 The maximum amplitude of these two pertubations and the value of X_T were taken as independent variables A multidimensional surface fit was carried out in the C_D, X_T, $\Delta y_{1_{max}}$, and $\Delta y_{2_{max}}$ space, using the form

$$C_D = C_0 + C_1L_1 + C_2L_2 + C_3L_3 + C_{11}L_1^2 + C_{22}L_2^2 + C_{33}L_3^2 + C_{12}L_1L_2 \quad (2)$$

where

$$\begin{aligned} \Delta y_{1_{max}} &= a_1 + b_1L_1 \\ \Delta y_{2_{max}} &= a_2 + b_2L_2 \\ X_T &= a_3 + b_3L_3 \end{aligned} \quad (3)$$

and the L_1, L_2, and L_3 are "reduced" variables as described in Ref 1 The physical variable $\Delta y_{1_{max}}$ is a linear function only of L_1; $\Delta y_{2_{max}}$ of L_2; and X_T of L_3 To determine the multidimensional surface fit, a 3 × 3 Latin Square was used This square, given in Ref 2, specifies nine different body shapes These nine shapes are shown in Fig 1 For each shape, the drag coefficient, based on the base area, was determined by using real gas blunt body and real gas method-of-characteristics computer programs A least squares surface fit then provided the values of the coefficient in Eq (2)

After determining the coefficients of Eq (2), a check of the surface fit was performed by evaluating Eq (2) for each test case Table 1 lists drag coefficients given by the computer programs, ratio of C_D to C_D for body 5 (the "basic" body), and the C_D value predicted by Eq (2) A very satisfactory fit is seen

The conditions for minimum drag, from Eq (2), are now

$$\begin{aligned} \partial C_D/\partial L_1 &= C_1 + 2C_{11}L_1 + C_{12}L_2 = 0 \\ \partial C_D/\partial L_2 &= C_2 + 2C_{22}L_2 + C_{12}L_1 = 0 \\ \partial C_D/\partial L_3 &= C_3 + 2C_{33}L_3 = 0 \end{aligned} \quad (4)$$

Using the numerical values for the coefficients as obtained by the multidimensional surface fit and solving system (4)

Table 1 Surface fit results

Body	C_D wave	C_{D_i}/C_D, case 5	C_D, Eq (2)
1	0 03864	1 038	0 03859
2	0 03716	0 999	0 03721
3	0 06443	1 732	0 06443
4	0 03824	1 028	0 03829
5	0 03721	1 000	0 03721
6	0 04821	1 296	0 04816
7	0 05061	1 360	0 05061
8	0 03749	1 006	0 03744
9	0 04865	1 307	0 04869

for the L_k's for minimum drag, the physical variables for minimum drag are found to be

$$\begin{aligned} \Delta y_{1_{max}} &= -0\ 0064 \\ \Delta y_{2_{max}} &= +0\ 0074 \\ X_T &= 0\ 00275 \end{aligned}$$

This minimum drag body is compared with the basic body in Fig 2 By Eq (2), the minimum C_D is

$$C_{D_{minpredict}} = 0\ 03182$$

From Table 1, the basic body drag coefficient is seen to be 0 03721 Thus, a drag reduction of 0 00558 (or 15%) has been achieved

By using the computer programs to determine the exact flow field about the minimum drag body, the drag coefficient was found to be

$$C_{D_{mincal}} = 0\ 03163$$

which equals 99 4% of predicted value

The agreement here is excellent in spite of the fact that $X_T = 0\ 00275$ represents an extrapolation of the calculated data (The problems were done within the limits of $0\ 025 \leq X_T \leq 0\ 075$) If wide differences exist between the calculated and predicted values for the minimum, the calculated body can be taken as the basic body, and another set of smaller pertubations can be used to determine the variation of C_D in this new local region By refining the "mesh" size in the physical variables, any desired accuracy can be obtained

The process just discussed is very flexible For example, should the minimum drag body having the sphere tangency point at $X_T = 0\ 05$ be desired, the last equation of system (4) is ignored and the first two are solved for L_1 and L_2 In this particular case the L_1, L_2 values are the same with or without constraints on the nose size The predicted value of C_D is $C_{D_{p\ edict}} = 0\ 03714$ The calculated value is $C_{D_{cal}} = 0\ 03717$ (= 100 1% of predicted value)

The variation of wave drag with nose radius for a $\frac{3}{4}$ power-law body is illustrated in Fig 3 A minimum does appear at $X_T = 0\ 00275$, but does not represent a significant improvement over the $\frac{3}{4}$ power-law body alone This result is in qualitative agreement with the experimental results of Ref 3 However, the skin-friction contribution that has been neglected here could significantly affect the results

Reference 4 shows that, for the optimum body when using a modification of Newtonian flow theory, $C_Df^2 = \frac{27}{64} = 0\ 422$, where f is the body fineness ratio L/D

The optimum body generated here has a predicted minimum drag parameter of $C_Df^2 = 0\ 510$ (predicted), and the

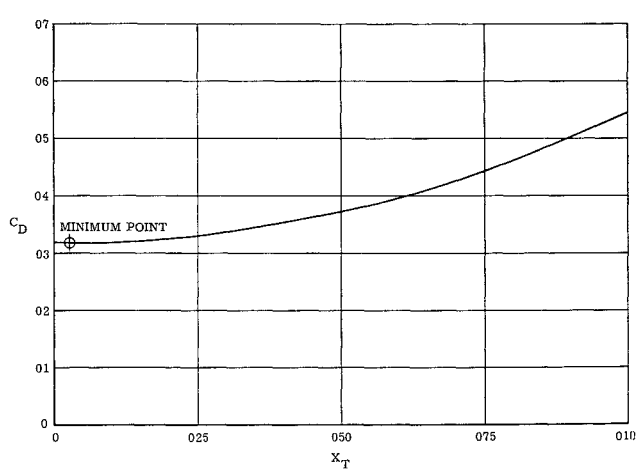

Fig 3 Variation of C_D with X_T for $\frac{3}{4}$ power-law body; $M = 7$, h = sea level

calculated value was found to be $C_D f^2 = 0\ 506$ (calculated)

The factor $\frac{2}{64}$ was derived assuming bodies with vanishingly small blunt noses The case considered here obviously departs from this assumption Reference 1 shows that the optimum value of $C_D f^2$ is a function of Mach number and fineness ratio

The work previously discussed was all carried out under the assumption of inviscid flows Reference 5 discusses the influence of skin friction on the body minimum drag although using several simplifying assumptions The process used in this note can be used to determine the exact viscid plus inviscid minimum drag shapes merely by adding an accurate viscous program to the process of calculating the individual body drags

References

[1] Powers, S A , "Minimum drag bodies of revolution by exact methods," NOR 63-156 Northrop Corp , Norair Div (September 1963)

[2] Powers, S A , "Drag minimization using exact methods," NOR-63-162, Northrop Corp , Norair Div (September 1963)

[3] Sommer, S C and Stark, J A , "The effect of bluntness on the drag of spherical-tipped truncated cones of fineness ratio 3 at Mach numbers 1.2 to 7 4, ' NACA RM A52B13 (1952)

[4] Miele, A , "Optimum slender bodies of revolution in Newtonian flow," Flight Sciences Labs TR 56, Boeing Scientific Research Labs (April 1962)

[5] Miele, A and Cole, J , "A study of optimum slender bodies in hypersonic flow with a variable friction coefficient," Flight Sciences Labs TR 66, Boeing Scientific Research Labs (January 1963)

Variation in Buckle Shape in Cylindrical Shells under External Pressure and Axial Load

W H Horton* and S C Durham†

Stanford University, Stanford, Calif

THE behavior of cylindrical shells under the combined action of internal pressure and axial compression has been studied, both theoretically and experimentally, by many investigators Prescott,[1] analyzing the problem on the basis of small displacement theory, reached the conclusion that there should be a parabolic increase of the critical buckling stress with the dimensionless parameter $\bar{p} = (p/E)(R/t)^2$, where p is the internal pressure, E is Young's modulus, R is the radius of the cylinder, and t is its wall thickness Flügge[2] re-examined the problem and after a comprehensive study reached the conclusion that internal pressure would have negligible effect on the buckling load These theoretical deductions are contradicted by experimental results Thus, Lo, Crate, and Schwartz[3] constructed a large-deflection theory, using the method of von Kármán and Tsien,[4] and showed that under these assumptions buckling load should increase with increasing values of $\bar{p}$ up to $\bar{p} = 0\ 169$ and thereafter remain constant Holmes[5] carried out a series of tests on the behavior of thin-walled cylinders under axial load and internal pressure The cylinders were made of aluminum alloy and were 3 ft in diameter and either 6 or 9 ft in length In his paper Holmes shows the buckle patterns that he obtained for various ratios of circumferential to longitudinal stress He observes that as this ratio increases there is a significant change in the aspect ratio of the buckles Fung and Sechler,[6] in their paper on the buckling of thin-walled circular cylinders under compression and internal pressure, make the same observation These experimenters used aluminum cylinders 3 5 in in diameter, 11 in in length, and having a wall thickness of one thousandth of an inch In a subsequent paper[7] the same authors show results obtained by Suer The same qualitative results are apparent

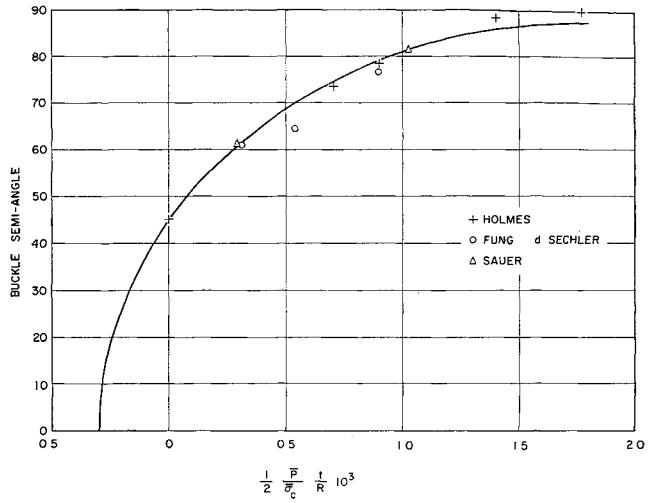

Fig 1 Variation of semiangle of buckle with pressure/stress ratio

We have examined the pictorial results given in the forementioned reports and have found that there is a distinct connection between the angle of buckle and the parameter p/σ_c The results of all these experimenters are plotted in Fig 1 It is seen from this figure that if we plot the semiangle of buckle against the ratio p/σ we obtain a smooth curve Complete details of the characteristics of the cylindrical shells and the measured semiangles of buckles are given in Table 1 We should emphasize that the various cylinders on which these observations were made were widely different with regard to the R/t ratio Moreover, some specimens were made from aluminum with a Young's modulus of 10×10^6 and others from steel with a Young's modulus of 30×10^6 The variation in L/D was, however, not great

The elliptic curve whose equation is given by

$$\theta = 41\ 665[1\ 17 + 1\ 8 \times 10^3(p/\sigma_c) - 0\ 25 \times 10^6(p/\sigma_c)^2]^{1/2} \text{ deg}$$

appears to be a good approximation to the relationship between the buckle semiangle θ and the pressure/stress ratio p/σ_c

Table 1 Listing of $\frac{1}{2}(\bar{p}/\bar{\sigma})(t/R) \times 10^3$ vs buckle semiangle

$\frac{1}{2}\frac{\bar{p}}{\bar{\sigma}}\frac{t}{R} \times 10^3$	Semiangle	Source
0 321	61°	Fung and Sechler (Suer), Fig 19a
1 026	81° 30′	Fung and Sechler (Suer), Fig 19b
0 311	60° 57′	Fung and Sechler, Fig 6
0 541	64° 32′	Fung and Sechler, Fig 7
0 900	76° 30′	Fung and Sechler, Fig 9
0 705	73° 30′	Holmes, Spec 6 (top)
0 903	78° 30′	Holmes, Spec 6 (bottom)
1 4	88° 30′	Holmes, Spec 5
1 77	90°	Holmes Spec 3

References

[1] Prescott, J , *Applied Elasticity* (Dover Publications, New York, 1946), Chap XVII

[2] Flügge, W , *Stresses in Shells* (Springer Verlag, Berlin, 1960), Chap VII

Received January 15, 1964 This work was performed for the U S Army Transportation Research Command under Contract DA 44-177-AMC-115(T)

* Director of Laboratories

† Major, U S Air Force